Large-scale molecular dynamics simulation of magnetic properties of amorphous iron under pressure

Pui-Wai Ma, W. C. Liu, and C. H. Woo[a)]
Department of Electronic and Information Engineering, The Hong Kong Polytechnic University, Hong Kong SAR, China

S. L. Dudarev
EURATOM/UKAEA Fusion Association, Culham Science Centre, Oxfordshire OX14 3DB, United Kingdom and Department of Physics, Imperial College, Exhibition Road, London SW7 2AZ, United Kingdom

We perform large-scale molecular dynamics simulations to study the magnetic properties of amorphous iron under pressure. Simulations, exceeding by at least two orders of magnitude those accessible to density functional calculations, use the recently developed magnetic interatomic potential for iron. The distributions of the size of atomic magnetic moments and parameters characterizing the structure of amorphous iron, such as radial distribution functions, are calculated as a function of the applied hydrostatic stress. As the density increases, there is a reduction in the magnitude of the mean magnetic moment of individual atoms, accompanied by the transformation of an increasing proportion of atoms from a magnetic to a nonmagnetic configuration. Beyond a critical density the proportion of nonmagnetic atoms increases sharply, yet homogeneously. The local magnetic moment of an atom correlates with the local Voronoi volume via a logarithmic relation. In addition, we observe a complex dependence of the local magnetic moment on the topological arrangement of neighboring atoms. © *2007 American Institute of Physics.*
[DOI: 10.1063/1.2715753]

I. INTRODUCTION

Amorphous materials are produced under nonequilibrium conditions inhibiting crystallization, such as rapid quenching from the melt.[1,2] The topological disorder constitutes a major factor that dominates properties of such materials. For example, amorphous magnets are soft magnetic materials which show easy magnetization due to the lack of long-range order and magnetocrystalline anisotropy.[2] Due to their noncrystalline structure they exhibit high electrical resistivity, high elastic limit, high magnetic permeability, and attractive corrosion resistance,[2,3] which make them useful for many applications, such as high-frequency devices, power distribution transformers, magnetomechanical transducers, and magnetoacoustic devices.[3]

Fabricating pure amorphous iron (μ-Fe) samples presented a number of practical challenges, and the properties of μ-Fe were extrapolated from those of amorphous systems with very high iron concentration.[4–6] The results, unfortunately, often proved ambiguous due to the presence of other components in the system. Pure μ-Fe in powder form can now be prepared with the sonochemical technique.[7–10]

Magnetism in the ground state of μ-Fe was studied almost exclusively using the electronic structure based methods. Kakehashi *et al.*[11–17] developed a treatment based on the degenerate-band Hubbard model and proposed that the ground state of μ-Fe was a spin glass. Kakehashi *et al.* investigated the magnetic phase diagram of μ-Fe as a function of temperature T and the d-electron occupation number N.

The phase diagram shows a paramagnetic, a collinear ferromagnetic, a noncollinear ferromagnetic, and a spin glass state. Turek and Hafner[18] performed electronic structure based molecular dynamics (MD) simulations using interatomic forces calculated using a method that combines the nearly free-electron and tight-binding-bond approximations. They also performed density functional calculations using 64-atom supercells in the linear-muffin-tin-orbital (LMTO) approximation. Upon compression, a sample of μ-Fe transforms from an inhomogeneous ferromagnetic state into an antiferromagnetic state and then further into a spin-glass state. Krauss and Krey[19] and Krey *et al.*[20] used a linear combination of atomic orbital (LCAO) approach combining the Slater-Koster parametrization of the hopping matrix elements of a tight-binding Hamiltonian with the Hartree-Fock treatment of on-site interaction between electrons, and generated the spin configurations for an amorphous cluster containing 54 atoms of iron. Initially, they adopted the conventional spin-up and spin-down approximations and discovered an inhomogeneous ferromagnetic state. Subsequently they generalized the treatment to noncollinear magnetic structures, and found asperomagnetic or speromagnetic energetically favorable configurations. Lorenz and Hafner,[21] using tight-binding parametrization of the Hubbard Hamiltonian, showed that as the density of the material increases, μ-Fe transforms from the ferromagnetic state into an asperomagnetic state and then into a speromagnetic state. Liebs *et al.*[22,23] performed *ab initio* calculations using supercells with 16 or 32 atoms. At low density, the system remained ferro-

---

[a)]Electronic mail: chung.woo@polyu.edu.hk

magnetic. At higher density, calculations showed the formation of noncollinear magnetic structures.

All the above calculations were based on density functional theory and/or the tight-binding Hubbard Hamiltonian. With more than 100 energy states per atom, the treatment of this Hamiltonian is computationally very demanding and in practice it proves difficult to investigate systems containing more than a few hundred atoms. Thus, the extension of *ab initio* approaches to the treatment of μ-Fe beyond the few hundred atoms scale is problematic. Although several semiempirical potentials for iron[24–27] were derived within the embedded atom method (EAM) formalism,[27–29] they have never been applied to the study of magnetic properties, since the magnetic contribution to the total energy of interaction between atoms cannot be separated. Ackland[30] proposed a way of including magnetic effects in a potential for a *d*-band magnetic metal, but he did not provide a parametrized scheme suitable for a practical simulation. Recently, using a combination of the Stoner "local band" treatment of ferromagnetism and the Ginzburg-Landau model, Dudarev and Derlet[31,32] (DD) developed a many-body "magnetic" interatomic potential for iron, in which the total energy of *N* atoms is written as

$$E_{\text{tot}} = \sum_{i}^{N} F[\rho_i] + \frac{1}{2} \sum_{i,j,i \neq j}^{N} V(r_{ij}), \tag{1}$$

where

$$F[\rho] = -A\sqrt{\rho} - \frac{B}{\ln 2}\left(1 - \sqrt{\frac{\rho}{\rho_c}}\right)\ln\left(2 - \frac{\rho}{\rho_c}\right)\Theta(\rho_c - \rho). \tag{2}$$

Here $V(r)$ is a pairwise repulsive potential term; A and B are constants; $\Theta(x)$ is the heaviside function; ρ is the effective electron density; ρ_c is a critical value of effective electron density at which magnetism vanishes. In addition to the usual many-body terms [the first term in (2)] describing collective interaction of an atom with its environment, this potential explicitly takes into account the local magnetic structure of the environment of a given atom and relates it to the effective local electron density [the second term in (2)], and includes the magnetic contribution to the total energy in the determination of the local atomic configuration. In the DD potential, the expression for the energy of interaction between atoms takes a convenient functional form similar to that of the embedded atom potential formalism, hence enabling fast evaluation of interatomic forces as well as the magnitude of the local magnetic moment of an atom in a large-scale MD simulation. As opposed to an electronic structure based order-N^3 approach, a MD simulation is an order-N method, making it possible to investigate processes on the scale that is many orders of magnitude greater. This capability is essential for large-scale simulations of magnetic materials. In this paper, using the magnetic potential, we investigate the relation between the local topological structure, magnetic properties of large samples of μ-Fe, and the magnetic/nonmagnetic transformation occurring under the applied external pressure. Within the DD approximation we are able to investigate how the magnitude of the local magnetic moment, but not its direction, depends on the parameters characterizing the structure, such as the local Voronoi volume of an atom and the number of the nearest neighbors. At this point we are not yet able to investigate the local orientation of magnetic moments, the treatment of which requires extension of the current methodology.

II. MD SIMULATION

The DD potential allows calculating the local magnetic moment of an atom (in units of μ_B) as well as the forces acting on it. Both quantities depend on the local environment of the atom. In our simulations, samples of μ-Fe of eight different densities were prepared by rapidly quenching atomic configurations from the melt. MD simulations of the heating and the subsequent quenching process were performed using canonical (*NVT*) ensembles for eight different mass densities, namely, 7.04, 7.46, 7.88, 7.92, 8.41, 8.95, 9.53, and 10.2 g/cm^3. The density of 7.88 g/cm^3 corresponds to the stress-free equilibrium configuration of bcc iron. By varying the density of the material we simulate the effect of applied hydrostatic stress. In each case, the system consists of approximately 16 000 atoms initially placed in a regular bcc lattice corresponding to a chosen value of mass density. The size of the simulation cell was approximately $60 \times 60 \times 60$ Å^3 in the $\langle 111 \rangle$, $\langle \bar{2}11 \rangle$, and $\langle 0\bar{1}1 \rangle$ directions, respectively. Periodic boundary conditions were applied in all three directions.

To simulate the formation of an amorphous structure by quenching a sample of liquid iron, we used two complementary methods. In the first method we followed Ref. 18 and fast quenched the system from the melt at the rate of 10^{15} K/s to 50 K, and then slowly quenched it to 4 K, and continued further to 0 K. In the second method we equated the velocity of each atom to zero repeatedly at every time step of a MD simulation and effectively followed the steepest descent trajectory in the phase space for the entire duration of the simulation of the order of 1 ns. We found that we were able to achieve better relaxed configurations using the second method, with the maximum remnant force reduced to less than 10^{-4} eV/Å, which is an order of magnitude lower than that found using the first method. The results obtained using the two methods are very similar, and in what follows we only describe structures simulated using the second method.

III. RESULTS AND DISCUSSIONS

The topological structure of the atomic arrangement in an amorphous material is generally explained in terms of dense random packing[33,34] and is best described by the radial distribution function (RDF) $g(r)$. Experimentally, the RDF of μ-Fe has only been investigated for thin films and powder samples. It is probably one of the most significant and interesting properties of pure μ-Fe studied both experimentally[9,33,34] and by computer simulation.[35,36]

A typical plot of the RDF obtained in our simulations is shown in Fig. 1 for the density of 7.88 g/cm^3. The blue bars represent the RDF of the corresponding perfect bcc lattice up to the fifth nearest neighbor, with the density of the first
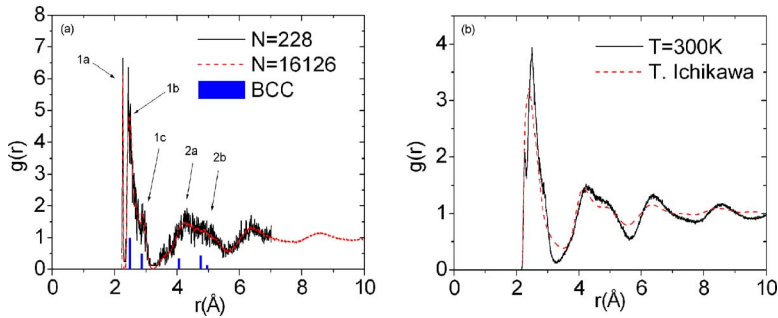
FIG. 1. (Color online) Radial distribution function (RDF) $g(r)$ of amorphous iron with density $=7.88$ g/cm^3 (a) at $T=0$ K and No. of atoms$=288$ and 16 126. The blue bars represent the RDF of the corresponding perfect bcc lattice up to fifth nearest neighbors, with the density of first nearest neighbor normalized to 1. (b) At $T=300$ K, No. of atoms$=16$ 126, and experimental data from Ichikawa (Ref. 33).

nearest neighbor normalized to one. It can be seen that instead of discrete values found for a perfect crystal lattice, distances between neighboring atoms in an amorphous metal are statistically distributed and showed up as broadened peaks. As indicated, the peaks in the RDF of μ-Fe are labeled 1a, 1b, 1c, 2a, and 2b. Their presence is independent of the size of the simulation cell. The 1a peak is below 2.31 Å, the 1b and 1c peaks are between 2.31 and 3.21 Å. The three peaks merge at 300 K [Fig. 1(b)] showing good agreement with experimental data. The splitting of the second peak (2a and 2b), with 2a peak higher than the 2b peak was proposed to serve as evidence for the formation of an amorphous state.[33] We observe good correlation between the positions of the 1b, 1c, 2a, and 2b peaks in μ-Fe and those of bcc-Fe. On the other hand, there is no such correspondence for the 1a peak. Due to the difficulty with resolving such a narrow peak in finite temperature data, it may be experimentally undetectable even if it existed. Maeda and Takeuchi[35] reported a similar observation of a narrow peak in the RDF, but attributed their finding to an artifact of the Johnson potential. In another calculation using *ab initio* MD,[18] the resulting RDF of μ-Fe did not show the 1a peak. At the same time, the *ab initio* MD simulations[18] did not show the splitting of the second peak either, whereas this should be expected to occur in a real amorphous structure. The relatively low level of resolution of RDF found in *ab initio* MD simulations is

likely attributable to the small size of the simulation cell. The RDF calculated for other amorphous metals[37–40] also shows only a single broad peak, without the sharp 1a peak. The fact that *ab-initio* calculations of self-interstitial defect structures in crystalline bcc iron (see below) show that atoms in the core of a defect approach each other as close as 1.95 Å suggests that clusters of atoms separated by very small distances may actually form in amorphous iron.

Figures 2(a) and 2(b) show the RDFs and changes in the structure of the 1a peak for a range of varying densities. The most prominent feature that we note is the small width ($<\sim 0.01$ nm) of the 1a peak, which remains sharp independently of the changes in the density of the material. This probably indicates that neighboring atoms corresponding to this peak are linked into clusters by bonds with a well-defined bond length. As the density increases, the 1a peak grows taller and shifts toward shorter interatomic separation distances, suggesting that the proportion of clustered atoms increases. The increase in the density does not alter the low cutoff value of the RDF that still remains at 2.31 Å. Figure 2(c) shows the corresponding behavior of the 1b and 1c peaks, both of which shrink as the density increases. Figures 2(b) and 2(c) together show that as the density increases, there is a reduction in the proportion of atoms with the neighboring environment of an approximate bcc structure, to
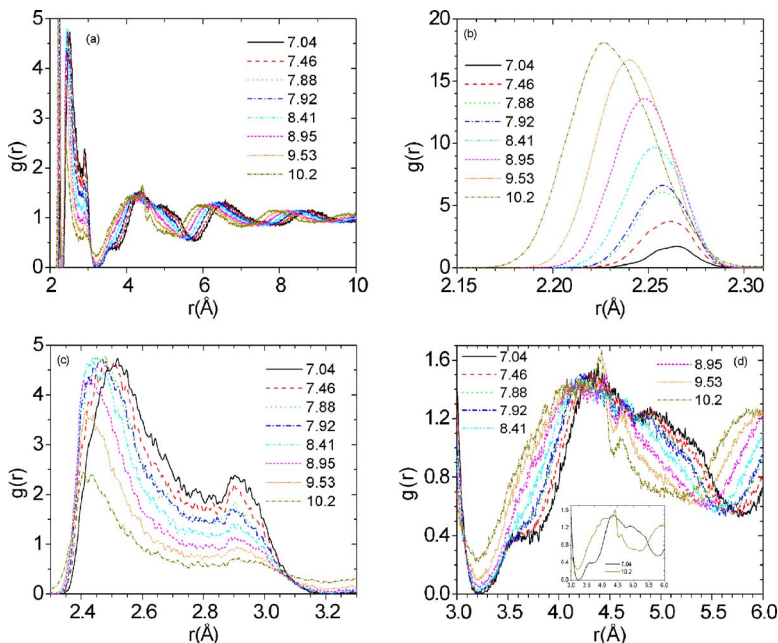

FIG. 2. (Color online) Radial distribution function (RDF) $g(r)$ of amorphous iron at different densities. (a) 2 Å$<r<$10 Å, (b) 2.15 Å$<r<$2.31 Å, (c) 2.3 Å$<r<$3.3 Å, and (d) 3.0 Å$<r<$6.0 Å.
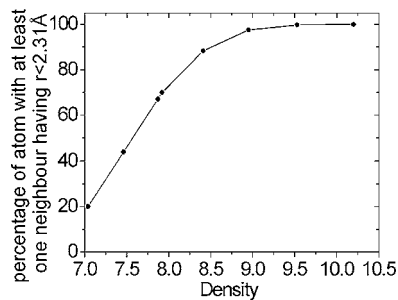
FIG. 3. Percentage of atoms for various densities with at least one neighbor with a separation of less than 2.31 Å.

feed the simultaneous growth of the proportion of clustered iron atoms. Figure 2(d) shows the behavior of the 2a and 2b peaks. Despite similar positions [see Fig. 1(a)], these peaks do not correspond to the third to fifth nearest neighbors of the bcc lattice. Indeed, these peaks can be well explained in terms of conventional dense random packing.[33,34] As the density increases, there is a general shift of the 2a and 2b peaks to smaller interatomic separations, accompanied by changes in the peak structure. It evolves from a structure formed by a superposition of two broad peaks to the one with a single broad peak and two superimposing sharp peaks located at around 4.40 and 4.61 Å. Smoothened lines for 7.04 and 10.2 g/cm^3 are shown in the inset of Fig. 2(d). According to Figs. 2(a)–2(d), the effect of an applied hydrostatic stress on the topological structure of the atomic environment of μ-Fe extends at least to the fifth nearest neighbor distance. Figure 3 shows that the percentage of atoms with at least one neighbor at interatomic separation smaller than 2.31 Å increases monotonically as a function of density.

To assess the accuracy of simulations performed using the DD potential against *ab initio* calculations, in Fig. 4(a) we show the structure and the magnitude of magnetic moments calculated using density functional calculations[41] compared with those evaluated using the magnetic interatomic potential[31,32] [Fig. 4(b)]. Comparison of structures in Figs.

4(a) and 4(b) shows that the positions of atoms as well as the magnitude of magnetic moments predicted by the DD potential agree satisfactorily with those found in *ab initio* calculations. The self-interstitial 110 dumbbell configuration shown in Fig. 4 represents the most energetically stable, as well as one of the most strongly distorted structures occurring in bcc iron. The fact that this structure is well described by the semiempirical magnetic potential used in this work suggests that the structures and magnetic configurations described below are representative of those of μ-Fe.

The calculated probability distribution of magnetic moments (MMD) shown in Fig. 5(a) exhibit a reduction in the mean magnetic moment and broadening of its probability distribution as a function of mass density of μ-Fe. This trend agrees very well with results reported in the literature (see, e.g., Fig. 2 of Ref. 18). The large scale of our simulations allows better statistical representation of data and offers clearer view of the trend relating the density of the material and the magnitude of the magnetic moment. Figure 5(b) shows the proportion of nonmagnetic iron atoms plotted as a function of density, indicating that μ-Fe remains magnetic at 0 K until the density reaches 8.41 g/cm^3, beyond which the proportion of nonmagnetic atoms increases sharply and the sample progressively loses its magnetic properties. At the density of 10.2 g/cm^3, practically all the atoms become nonmagnetic, completing the magnetic/nonmagnetic transition driven by the increasing hydrostatic pressure. The corresponding pressure is shown in the inset of Fig. 5(b). The pressure is calculated according to virial theorem. At the density of 8.95 g/cm^3, the pressure is ∼12.7 GPa. We can also observe a linear regime in the pressure-density relationship for smaller pressures before the sample gradually loses its magnetism.

Figures 6(a) and 6(b) show the mean and the standard deviation of the MMD as a function of mass density. The figures show plots comparing cases where the nonmagnetic atoms were included or excluded from statistical analysis. We see that although there is an overall reduction in the
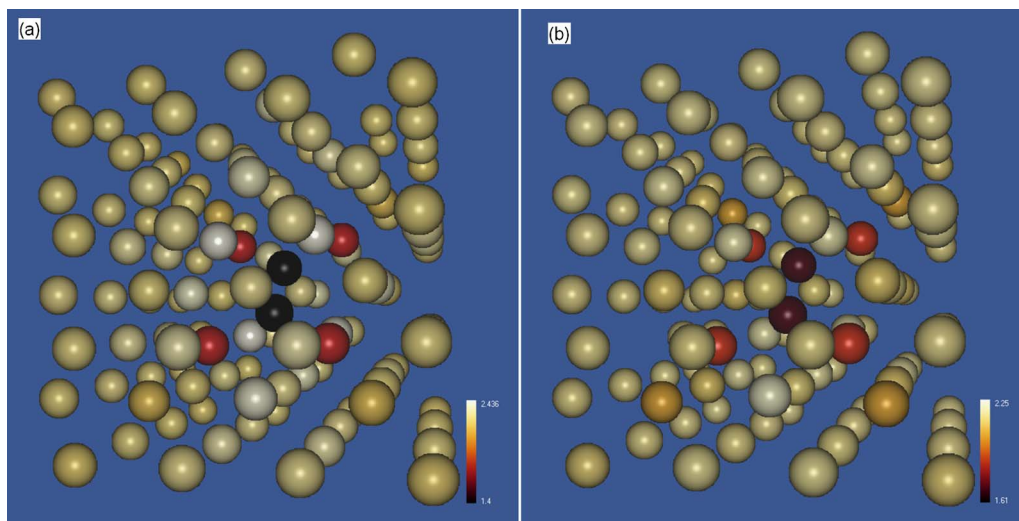

FIG. 4. (Color online) (a) Atomic configuration and magnetic moments for the 110 dumbbell configuration in bcc iron calculated using density functional theory and (b) the same configuration modeled using the magnetic interatomic potential. The differences between (a) and (b) are associated with the approximate treatment of interatomic forces and magnetic moments within the magnetic interatomic potential formalism.
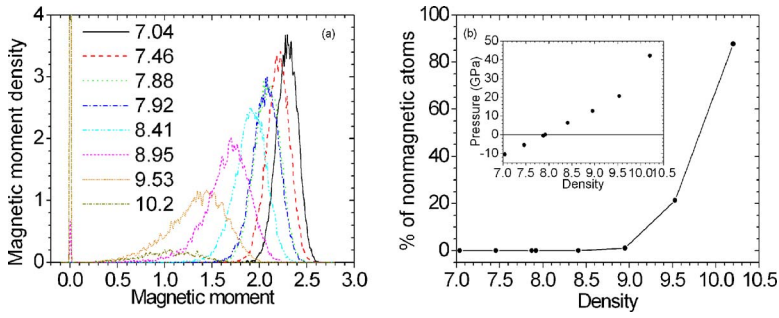
FIG. 5. (Color online) (a) Magnetic moment density vs magnetic moment at different densities. (b) Percentage of nonmagnetic atoms vs density.
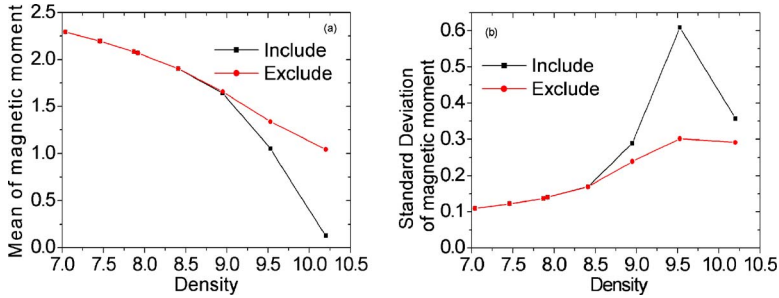

FIG. 6. (Color online) The mean (a) and standard deviations (b) of magnetic moment vs the number density including/excluding atoms with magnetic moment equals to zero.
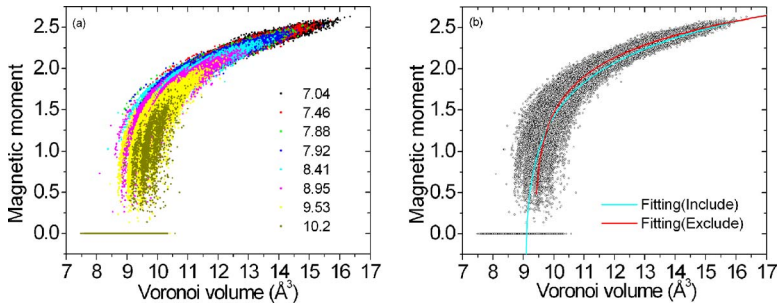

FIG. 7. (Color online) (a) Magnetic moment vs Voronoi volume at different densities. (b) The magnetic moment fitted as a function of the Voronoi volume. The blue line represents fitting to all atoms and the red line represents fitting without the nonmagnetic atoms.
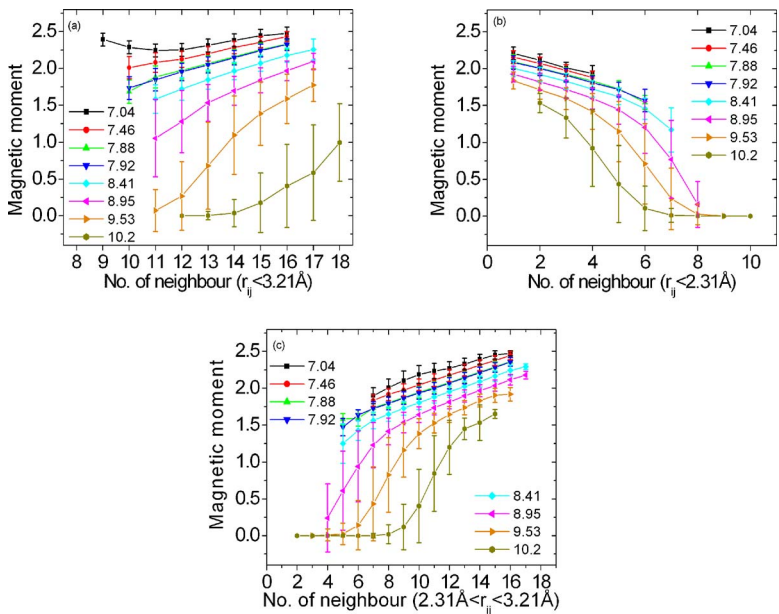

FIG. 8. (Color online) The mean of magnetic moment vs number of neighbors for (a) $r_{ij} < 3.21$ Å, (b) $r_{ij} < 2.31$ Å, and (c) 2.31 Å $< r_{ij} < 3.21$ Å.

magnetic moment of iron atoms as a function of density, the disappearance of magnetism with increasing density is primarily the result of the sharp increase in the fraction of nonmagnetic atoms. The corresponding standard deviation of the MMD in Fig. 6(b) shows a turning point at the density of 9.53 g/cm^3, where the proportion of magnetic and nonmagnetic atoms is comparable, and it drops again at the density of 10.2 g/cm^3 where the majority of atoms are nonmagnetic. Figure 6 shows that μ-Fe loses its magnetic properties gradually as the hydrostatic pressure increases. Similarly to the situation occurring in the core of the self-interstitial defect shown in Fig. 4(a), the origin of the magnetic/nonmagnetic transition is driven by mechanical effects (increase of hydrostatic pressure) and is dissimilar to the temperature-driven order-disorder transition occurring in a ferromagnetic material at the Curie temperature.

In Fig. 7, the magnitude of the magnetic moment of an atom is plotted against its Voronoi volume. The positive correlation seen for all densities does not fully agree Turek and Hafner's result[27] suggesting that the local volume/magnetic moment correlation ceases to exist in the high density limit. We observe only a reduction in this correlation at high pressure, hence making our simulations more consistent with the picture proposed by Krauss and Krey.[28] The relation between the absolute value of magnetic moment M and the Voronoi volume V in Fig. 6 can be represented by a best-fit equation $M=a\ln(V-c)+b$. The blue line is fitted using all the atoms in the simulation cell. The fitted values are $a=0.591\,47 \pm 0.001\,25$, $b=1.422\,86\pm0.001\,32$, $c=9.002\,75\pm0.000\,54$, and value of the correlation coefficient is 0.801 72. The orange line is fitted with the nonmagnetic atoms excluded, and the corresponding fitting parameters are $a=0.484\,79 \pm 0.000\,84$, $b=1.659\,11\pm0.000\,86$, $c=9.3355\pm0.000\,54$ with the correlation coefficient of 0.821 68. The magnetovolume relation for μ-Fe is close to that for the antiferromagnetic state in fcc iron, which is consistent with the close-packed structure of this phase.[11] At the same time we observe that volume is not the only factor that determines the magnitude of magnetic moment. This is evident from the spatial fluctuations of magnitudes of magnetic moments of individual atoms, which can be very large, particularly near the Voronoi volume of 9.5 Å^3 per atom. In this case even for atoms occupying the same Voronoi volume, the magnetic moment can vary from $0\mu_B$ to nearly $2\mu_B$.

To analyze these fluctuations further, in Fig. 8 we plotted the mean value of the local magnetic moment as a function of the number of neighbors within the radius of 3.21 Å. Intuitively, one would expect that as the number of neighbors increases, the mean magnetic moment would decrease due to the higher electron density on an atom. However, Fig. 8 shows a surprising increase in the mean magnetic moment as the number of neighbors increases. We further examine the respective situations in the 1a, 1b, and 1c peaks separately, and find that in the 1a peak, the magnetic moment indeed decreases as the number of neighbors increases. In the 1b and 1c peaks, on the other hand, the magnetic moment increases with the increasing number of neighbors. Thus, we are forced to also consider the relationship between the

Voronoi volume and the number of neighbors of a given atom to arrive at a consistent picture of the magnetic/nonmagnetic transition.

In Fig. 9, we plot the number of neighbors versus the Voronoi volume. The figure shows the expected decrease in the Voronoi volume as a function of the number of neighbors in the 1a peak, and the opposite trend for the 1b and 1c peaks. We suppose that owing to their small interatomic separation, iron atoms forming the 1a peak develop local structures characterized by a specific bond length, so that as the number of neighbors increases, the volume occupied by each atom is reduced. On the other hand, atoms in the 1b and 1c peaks are more loosely bonded via the usual metallic bonding mechanism. Atomic positions here are more flexible, i.e., they are energetically less sensitive to the exact positions of atoms. An additional atom keeping its atomic volume tends to repel other atoms and this causes the Voronoi volume of the center atom to increase, resulting in a larger size of the local magnetic moment.

In Fig. 10(a), we show the statistical distribution of the number of neighbors corresponding to various densities. The curves represent the best fit to Gaussian distributions. The close-to-perfect correlation means that the distribution of the number of neighbors in amorphous iron is random. The mean number of neighbors versus density shown in Fig. 10(b) exhibits a linear relationship $\bar{N}=a+b\rho$ between the mean number of neighbor $\bar{N}$ and the density ρ, with $a=8.456\,66 \pm0.178\,89$, $b=0.586\,13\pm0.021\,09$, and the correlation coefficient of $R^2=0.996\,14$. Using Johnson's potential, Srolovitz *et al.*[36] observed that structures with 13 neighbors form the largest part of the population. This is similar to our results shown in Fig. 10(a).

Figure 11(a) shows the magnitude of magnetic moment as a function of the percentage fluctuation of the interatomic separation $\Delta^{1/2}$. In comparison with Fig. 5 of Ref. 14, the fluctuation of our result is about twice the value reported there. According to the results shown in Fig. 11(b) the fluctuation varies almost linearly as a function of density.

Figure 12 shows atomic structures and color-coded magnetic moments of atoms in the simulation cell displayed for several values of the mass density of the material. As the density increases, the number of nonmagnetic (dark) atoms increases and beyond a critical value of mass density the material completely loses its magnetic properties. The structures shown in Fig. 12 illustrate the fairly complex nature of the magnetic/nonmagnetic transition occurring in μ-Fe under applied pressure. The origin of the transition from a magnetic to a nonmagnetic state is associated with the local widening of the electronic d band due to the increase of the local hopping integrals, and the resulting violation of the local Stoner criterion for magnetism.[31,32] The increase of the amplitude of the local hopping integrals is due to the local deformation of atomic structure such as that occurring in the core region of a self-interstitial atom defect shown in Fig. 4. In this regard the mechanism of the magnetic/nonmagnetic transition observed in our simulations is entirely different from that of the order-disorder ferro-/paramagnetic transition occurring in crystalline bcc iron at the Curie temperature.
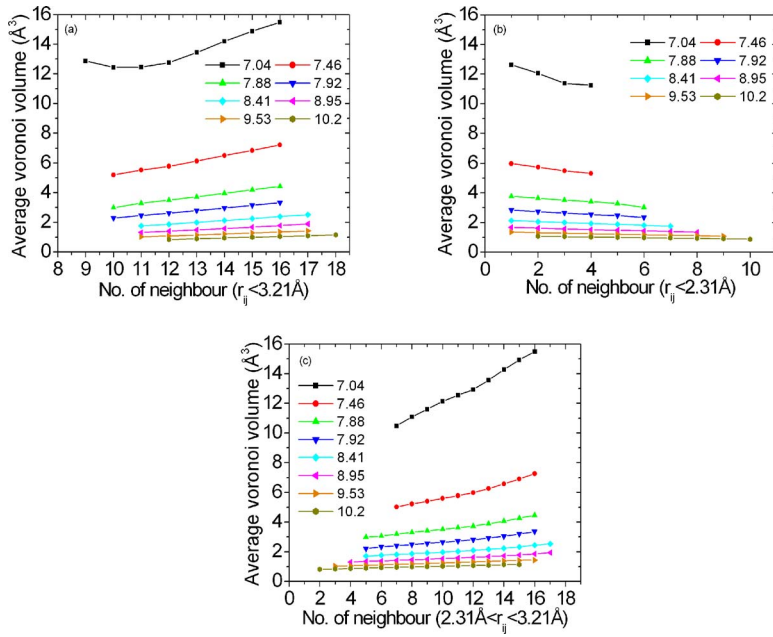
FIG. 9. (Color online) Average Voronoi volume vs number of neighbors (a) $r_{ij} < 3.21$ Å, (b) $r_{ij} < 2.31$ Å, and (c) 2.31 Å $< r_{ij} < 3.21$ Å.
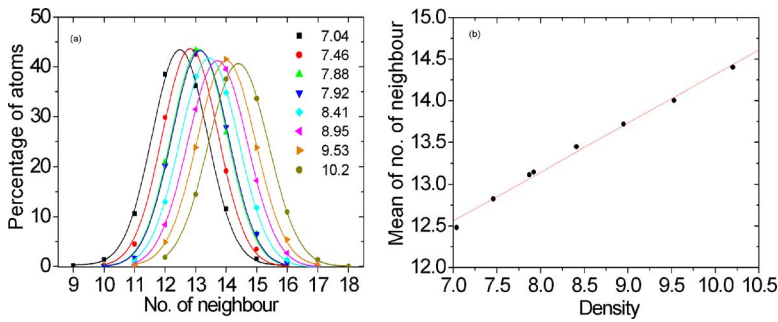

FIG. 10. (Color online) (a) The distribution of number of nearest neighbors at different densities. (b) The mean of the number of neighbors vs density. Red line is the linear fitting.
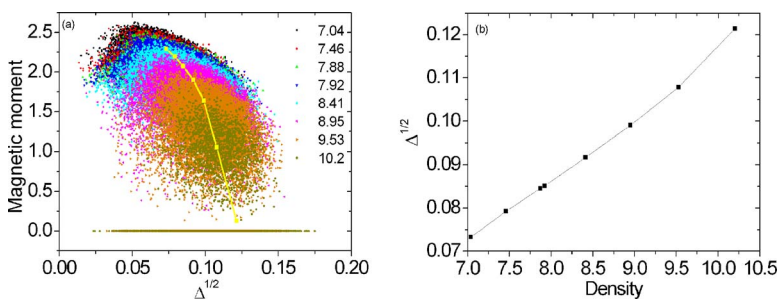

FIG. 11. (Color online) (a) The local magnetic moment vs the local fluctuation of the interatomic separations at different densities; the yellow dot is the mean of magnetic moment vs the average fluctuations of interatomic separations $\Delta^{1/2} = \langle (\delta R)^2 \rangle^{1/2} / \langle R \rangle$. (b) The average fluctuations of interatomic distance vs the number densities
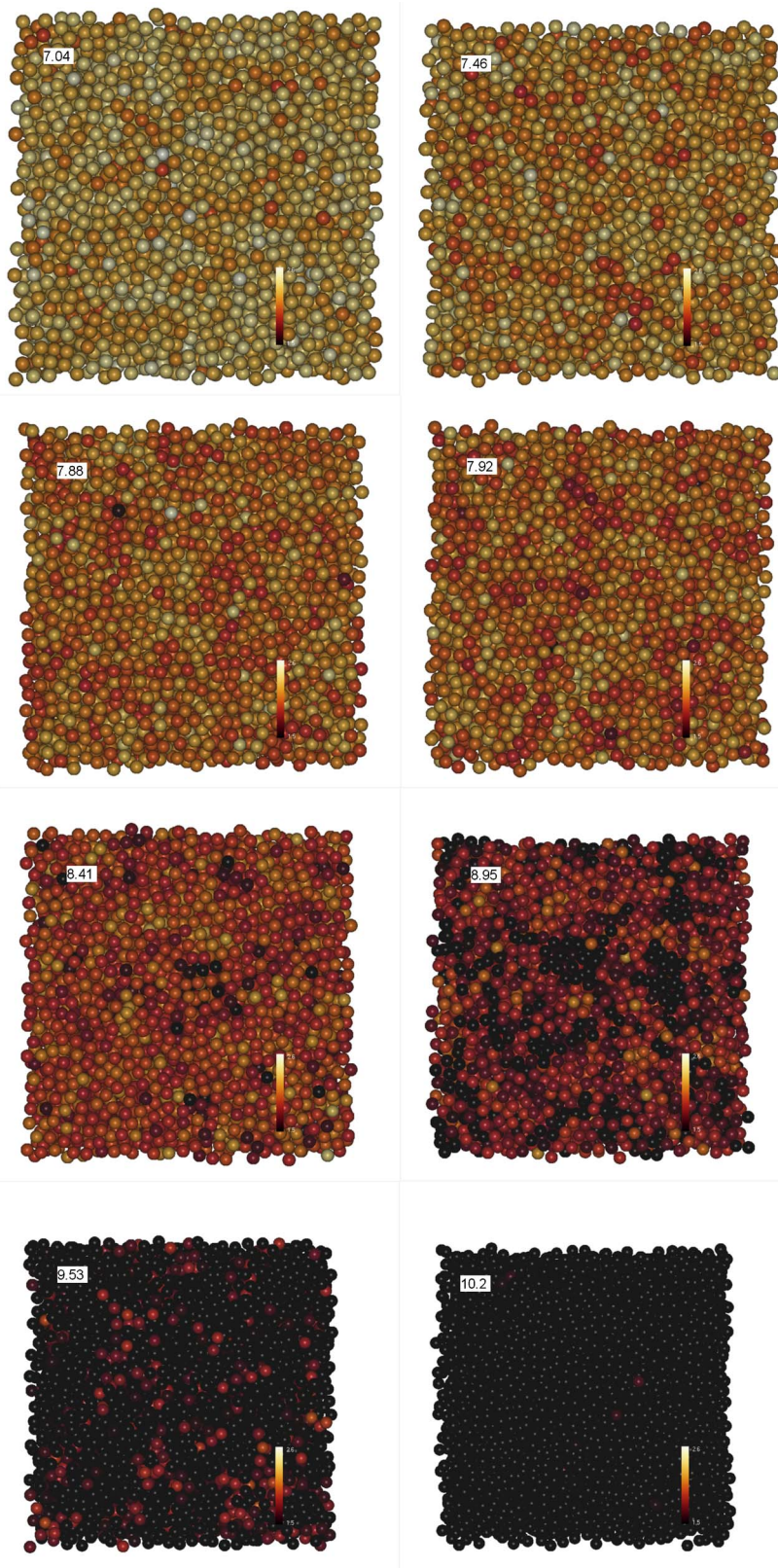
FIG. 12. (Color online) Atomic structures and magnetic moments of atoms simulated using the magnetic potential for systems containing approximately 16 000 atoms for different values of mass density. Darker color represents atoms with lower magnetic moments. The figure illustrates the gradual nature of the magnetic/nonmagnetic transition occurring in amorphous iron under increased external pressure.

There are two possible scenarios for the magnetic/nonmagnetic transition, namely, that it occurs either via inhomogeneous nucleation and growth of a small number of nonmagnetic clusters of atoms or via homogeneous nucleation driven by the uniform increase in the fraction of nonmagnetic atoms in the simulation cell. Our results offer support to the second scenario. Examination of three-dimensional magnetic structure of simulated configurations shows that the nonmagnetic atoms form largely disconnected clusters, with the loss of magnetic properties driven by local mechanical distortions. To verify this conclusion, we added a nonmagnetic 15-atom cluster at the center of the computational cell, and found that this cluster did not grow. Magnetism did not vanish through the growth of nonmagnetic is-

lands, and remained a fluctuating entity throughout the simulation. To what extent this picture is affected by the correlation between magnetic moments driven by interatomic exchange remains to be investigated.

IV. CONCLUSION

We performed large-scale molecular dynamics simulations to investigate magnetic properties of amorphous iron under external pressure. The simulations were preformed using the recently developed magnetic interatomic potential. We found that as the density of the material increased, an increasing fraction of atoms became nonmagnetic. Above a critical density the fraction of nonmagnetic atoms increased sharply, yet homogeneously. The magnetic/nonmagnetic transition occurred continuously and homogeneously, and did not involve nucleation and growth of individual nonmagnetic clusters. The local magnetic moment density is correlated with the Voronoi volume per atom, and the relation between the two follows a logarithmic law. We also find evidence for the significant role played by the local atomic environment.

ACKNOWLEDGMENTS

[1]T. Kaneyoshi, *Amorphous Magnetism* (CRC, Boca Raton, FL, 1984), Chaps. 1 and 2.
[2]R. C. O'Handley, *Modern Magnetic Materials: Principles and Applications* (Wiley, New York, 2000), Chaps. 10 and 11.
[3]T. Egami, Rep. Prog. Phys. **47**, 1601 (1984).
[4]G. Xiao and C. L. Chien, Phys. Rev. B **35**, 8763 (1987).
[5]G. Xiao and C. L. Chien, J. Appl. Phys. **61**, 3246 (1987).
[6]D. H. Ryan, L. X. Liao, and Z. Altounian, Solid State Commun. **66**, 339 (1988).
[7]K. S. Suslick, S.-B. Choe, A. A. Cickhowlas, and M. W. Grinstaff, Nature (London) **353**, 414 (1991).
[8]M. W. Grinstaff, M. B. Salamon, and K. S. Suslick, Phys. Rev. B **48**, 269 (1993).
[9]R. Bellissent, G. Galli, M. W. Grinstaff, P. Migliardo, and K. S. Suslick, Phys. Rev. B **48**, 15797 (1993).
[10]G. J. Long *et al.*, Phys. Rev. B **57**, 10716 (1998).
[11]M. Yu and Y. Kakehashi, Phys. Rev. B **49**, 15723 (1994).
[12]Y. Kakehashi and M. Yu, Phys. Rev. B **50**, 6189 (1994).
[13]Y. Kakehashi and M. Yu, J. Magn. Magn. Mater. **140**, 255 (1995).
[14]Y. Kakehashi, T. Uchida, and M. Yu, Phys. Rev. B **56**, 8807 (1997).
[15]Y. Kakehashi, S. Akbar, and N. Kimura, Phys. Rev. B **57**, 8354 (1998).
[16]Y. Kakehashi and T. Uchida, J. Phys.: Condens. Matter **12**, 8683 (2000).
[17]T. Uchida and Y. Kakehashi, Phys. Rev. B **64**, 054402 (2001).
[18]I. Turek and J. Hafner, Phys. Rev. B **46**, 247 (1992).
[19]U. Krass and U. Krey, J. Magn. Magn. Mater. **98**, L1 (1991).
[20]U. Krey, U. Krauss, and S. Krompiewski, J. Magn. Magn. Mater. **103**, 37 (1992).
[21]R. Lorenz and J. Hafner, J. Magn. Magn. Mater. **139**, 209 (1995).
[22]M. Libes, K. Hummler, and M. Fähnle, Phys. Rev. B **51**, 8664 (1995).
[23]M. Libes and M. Fähnle, Phys. Rev. B **53**, 14012 (1996).
[24]M. W. Finnis, *Interatomic Forces in Condensed Matter* (Oxford University Press, New York, 2003).
[25]G. J. Ackland, D. J. Bacon, A. F. Calder, and T. Harry, Philos. Mag. A **75**, 713 (1997).
[26]M. I. Mendelev, S. Han, D. J. Srolovitz, G. J. Ackland, D. Y. Sun, and M. Asta, Philos. Mag. **83**, 3977 (2003).
[27]M. W. Finnis and J. E. Sinclair, Philos. Mag. A **50**, 45 (1984).
[28]M. S. Daw and M. I. Baskes, Phys. Rev. Lett. **50**, 1285 (1983).
[29]M. S. Daw and M. I. Baskes, Phys. Rev. B **29**, 6443 (1984).
[30]G. J. Ackland, J. Nucl. Mater. **351**, 20 (2006).
[31]S. L. Dudarev and P. M. Derlet, J. Phys.: Condens. Matter **17**, 7097 (2005).
[32]P. M. Derlet and S. L. Dudarev, Prog. Mater. Sci. **52**, 299 (2007); UKAEA Fusion Report No. 530, 2006 (unpublished); available on www.fusion.org.uk
[33]T. Ichikawa, Phys. Status Solidi A **19**, 707 (1973).
[34]G. Shen, M. L. Rivers, S. R. Sutton, N. Sata, V. B. Prakapenka, J. Oxley, and K. S. Suslick, Phys. Earth Planet. Inter. **143**, 481 (2004).
[35]K. Maeda and S. Takeuchi, J. Phys. F: Met. Phys. **8**, L283 (1978).
[36]D. Srolovitz, K. Maeda, S. Takeuchi, T. Egami, and V. Vitek, J. Phys. F: Met. Phys. **11**, 2209 (1981).
[37]B. E. Clements and D. C. Wallace, Phys. Rev. E **59**, 2955 (1999).
[38]A. Posada-Amarillas and I. L. Garzón, Phys. Rev. B **53**, 8363 (1996).
[39]Q. X. Pei, C. Lu, and M. W. Fu, J. Phys.: Condens. Matter **16**, 4203 (2004).
[40]J. L. Feldman, N. Bernstein, D. A. Papaconstantopoulos, and M. J. Mehl, J. Phys.: Condens. Matter **16**, S5165 (2004).
[41]D. Nguyen-Manh (private communication).